IEEE Access
Multidisciplinary | Rapid Review | Open Access Journal

Received October 29, 2019, accepted November 19, 2019, date of publication November 29, 2019,
date of current version December 31, 2019.

Digital Object Identifier 10.1109/ACCESS.2019.2956846

New Reaching Law Control for Permanent Magnet Synchronous Motor With Extended Disturbance Observer

YAOQIANG WANG[1], (Member, IEEE), YUTAO FENG[1,2], XIAOGUANG ZHANG[3], (Member, IEEE), JUN LIANG[1,4], (Senior Member, IEEE), AND XIAN CHENG[1]

[1]School of Electrical Engineering, Zhengzhou University, Zhengzhou 450001, China
[2]AVIC Jonhon Optronic Technology Company, Ltd., Luoyang 471003, China
[3]Inverter Technologies Engineering Research Center of Beijing, North China University of Technology, Beijing 100144, China
[4]School of Engineering, Cardiff University, Cardiff CF24 3AA, U.K.

Corresponding author: Xian Cheng (chengxian@zzu.edu.cn)

This work was supported in part by the National Natural Science Foundation of China under Grant 51507155 and Grant 51877002, and in part by the Youth key Teacher Project of the Provincial Higher Educational Institution of Henan under Grant 2019GGJS011.

ABSTRACT In order to improve the anti-disturbance performance of permanent magnet synchronous motor (PMSM) servo system, a sliding-mode control strategy using a new reaching law (NRL) is proposed. The NRL incorporates power term and switching gain term of the system state variables into the conventional exponential reaching law (CERL), which can effectively suppress the sliding-mode chattering and increase the convergence rate of system state reaching sliding-mode surface. Based on this new reaching law, a sliding-mode speed controller (SMSC) of PMSM is designed. At the same time, to solve the chattering problem caused by the large sliding-mode switching gain, an anti-disturbance sliding-mode speed controller method with an extended sliding-mode disturbance observer (ESMDO), called SMSC+ESMDO method, is developed. The sliding-mode disturbance observer is designed to accurately estimate the motor speed and external load disturbances, and the disturbance estimator is used as a feed-forward to compensate the sliding-mode speed controller (SMSC) to improve the system robustness and reduce the system chattering. Simulation and experimental results show that the proposed compound sliding-mode control strategy can effectively improve the dynamic performance and robustness of the system compared with the PI controller.

INDEX TERMS Permanent magnet synchronous motor (PMSM), new reaching law, anti-disturbance sliding-mode speed controller (ADSMSC), extended sliding-mode disturbance observer, robustness.

NOMENCLATURE

s	Sliding-mode surface function.
$\varepsilon\mathrm{sgn}(s)$	Isokinetic reach term.
ks	Index reach term.
x	System state variable.
k_1	Switching gain.
k_2	Linear gain.
ε	Variable term coefficient.
δ	The thickness of the boundary layer.
J	The rotary inertia.
$u(t)$	Controller input.
$\theta(t)$	Position instruction.
$d(t)$	External disturbance.
$\theta_\mathrm{d}(t)$	Ideal position signal.
ω^*	Given reference speed.
ω	Actual feedback speed.
L	Equivalent inductance.
p	The number of poles of the motor.
B	The viscous friction coefficient.
$\dot{T}_\mathrm{L}$	The estimated load torque.
$R(t)$	System comprehensive disturbance.
l_r	The limit value of the system comprehensive disturbance.
T_e	Electromagnetic torque.

The associate editor coordinating the review of this manuscript and approving it for publication was Xiaoli Luan.

$r(\omega_e)$	The sliding-mode control rate of the observation error.
z	Observer gain.
e_ω	Motor speed observation error.
e_R	Motor disturbance observation error.
k_3	The sliding-mode switching gain.

I. INTRODUCTION

Permanent magnet synchronous motor (PMSM) has the advantages of simple structure, high power density and high efficiency. It has been widely used in high-precision CNC machine tools, robots, aerospace and other fields [1]. PMSM is a multi-variable, strong coupling, nonlinear and complex controlled object with variable parameters. Although the conventional PID control can meet the control requirements within a certain precision range, the linear controller has the problem of integral saturation, and is very sensitive to external disturbances and internal parameter changes. All these may make the control system deviate from the expected target and limits its application in high-performance control occasions [2]–[4].

To solve the above problems of conventional PID control, some modern control theories, such as fuzzy control [5], state feedback control [6], predictive control [7], internal model control [8], sliding-mode control (SMC) [9]–[11], and neural network control [12] have been proposed. Among them, SMC has many advantages, such as fast response, insensitive to corresponding parameter changes and disturbances, no on-line identification of the system, simple physical implementation, etc. and has been successfully applied in motor servo system [13]–[16]. In [17], sliding-mode control was applied to the sensor-less servo system of permanent magnet synchronous motor, which improved the control precision of the speed controller. In [18], a SMC based on a NRL was designed. The experimental results show that the robustness and the dynamic performance of the controlled system were improved. However, this reference does not take into account the effect of the switching function on chattering. In [19], based on a new sliding reaching law, a SMC was introduced into the vector control servo system with $i_d = 0$, which effectively improves the dynamic performance and robustness of the system.

However, practical applications show that when the system state variable reaches the sliding-mode surface along the trajectory, it is difficult to slide along the sliding-mode surface and converge to the equilibrium point, but constantly traverse both sides of the sliding-mode surface, which will inevitably lead to chattering [20]–[23]. Therefore, the suppression of chattering is the key to sliding-mode control research. Because the reaching law is directly related to the process of system state variable approaching sliding-mode surface, the chattering of sliding-mode can be effectively suppressed by designing the reaching law reasonably. In view of this, a terminal sliding-mode speed controller was proposed for PMSM [24], and a nonlinear term was introduced to the sliding-mode controller, which is effective to reduce the chatting and improve the convergence rate. In [25], authors presented some reaching laws, which can restrain chattering by gain decreasing or making the discontinuous gain a function of sliding-mode surface. Similarly, based on the NRL, a second-order sliding-mode controller for PMSM servo system was designed in [26]. The theoretical and simulation results show that the system could still meet the accuracy requirements under severe external disturbances. However, the design of the second-order sliding-mode control is complex, and it is difficult to achieve the desired control effect in practice.

Based on the above problems, a SMC strategy based on a NRL and disturbance observer is designed to obtain the auto-disturbance rejection ability to improve the robustness of the system. Firstly, based on the conventional exponential reaching law (CERL), power term and switching gain term of the system state variables are added to solve the contradiction between the system chattering and sliding-mode approaching speed. Then, to further improve the anti-disturbance ability of the servo system, an extended sliding-mode disturbance observer (ESMDO) is designed, which simultaneously takes the velocity and disturbance as the observation object, and compensates the observed disturbance to the sliding-mode speed controller. Finally, simulation and experimental results show that the proposed control strategy can effectively improve the dynamic characteristics and robustness of PMSM servo system.

The rest of this paper is organized as follows. In section II, the proposed NRL and its performance analysis are introduced. This part also gives the design of SMSC. In section III, the design process of ESMDO and ESMDO-based SMSC are given. In section IV, the ESMDO-based SMSC is tested on PMSM experiment platform, and the results are compared to the PI regulator. The final summaries of the paper are given in section V.

II. SLIDING-MODE CONTROLLER DESIGN

A. CONVENTIONAL EXPONENTIAL REACHING LAW AND ITS ANALYSIS

Generally, the design process of sliding-mode controller includes two steps: one is to select a reasonable sliding-mode surface, and the other is to design a reaching law to make the system state trajectory approach the sliding-mode surface under the action of reaching law. Among them, the reaching law can ensure the dynamic quality of the system through the process of approaching movement, that is, by choosing an appropriate reaching law, the system can have a larger reaching speed far from the switching surface, so as to improve the response of the controlled system, and when approaching the sliding-mode surface, its speed gradually reduces to zero to suppress chattering. Fig.1 shows how this mechanism works in the phase plane.

The form of CERL proposed by the famous expert Weibing Gao is shown in (1)

$$\frac{ds}{dt} = -\varepsilon \mathrm{sgn}(s) - ks, \quad \varepsilon > 0,\ k > 0 \tag{1}$$

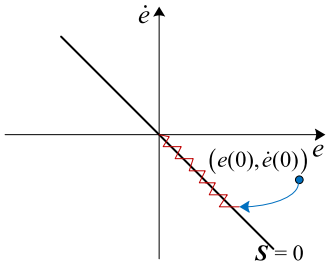

FIGURE 1. Sliding-mode mechanism in phase plane.

where s is a sliding-mode surface function; $\varepsilon \mathrm{sgn}(s)$ represents isokinetic reach term; ks represents index reach term;. For the CERL, it cannot reach the sliding-mode surface in a certain period of time. Therefore, the isokinetic reach term $\varepsilon sgn(s)$ is added to ensure that when s is close to 0, the arrival velocity is ε instead of 0.

In (1), when $s > 0$

$$\frac{ds}{dt} = -\varepsilon - ks \tag{2}$$

The reaching time can be obtained by integrating (2), with s(t)=0

$$t^* = \frac{1}{k}(\ln(s(0) + \frac{\varepsilon}{k}) - \ln\frac{\varepsilon}{k}) \tag{3}$$

It can be seen from (3) that the reaching speed increases with the k value. Therefore, in order to obtain a faster reaching performance, the value of k should be increased; however, increasing the value of k causes the speed to be too fast when reaching the sliding surface, which will increase the chattering level. Therefore, if the coefficient of the index item is set as a variable and its value is combined with the distance between the system state point and the sliding-mode surface, the contradiction caused by the k value selection can be solved. This also provides an idea for the NRL presented below.

B. THE PROPOSED NRL

In order to overcome the drawbacks of the CERL, a NRL is proposed in this paper, which is expressed as

$$\begin{cases} \dot{s} = -k_1 H(x)\,\mathrm{sign}(s) - k_2 |x|^{\alpha} \cdot s \\ H(x) = \dfrac{|x|}{|x| + \varepsilon} \\ \lim\limits_{t\to\infty} |x| = 0, \quad k_1 > 0,\ k_2 > 0,\ 0 < \alpha < 2 \end{cases} \tag{4}$$

where s represents the sliding-mode surface. x is the system state variable. k_1 is the switching gain. k_2 is a linear gain. $\varepsilon > 0$ is a variable term coefficient.

Compared with the CERL, the NRL introduces the variable gain term $H(x)$ and the power term of the system state variable $|x|^{\alpha}$. Among them, the variable gain term $H(x)$ gradually decreases and eventually converges to zero along with the system state approaching trajectory and finally reaches the sliding-mode surface, which ensures that the variable gain $k_1 H(x)$ remains smaller than the original switching gain k_1 throughout the approaching process, so the sliding-mode chattering can be effectively suppressed. In addition, the introduction of the system state variable $|x|^{\alpha}$ makes the system have a larger approaching speed at the initial approaching stage, and the system state $|x|$ gradually decreases and approaches zero at the sliding-mode surface, which makes the approaching speed of the system state converge to zero gradually when it reaches the sliding-mode surface. Therefore, NRL improves the shortage of conventional exponential reaching law.

Besides, the sign(s) function in the NRL can be replaced by the saturation function. For the reason of practical applications, the hysteresis of the switch in time and space and the inherent inertia of the system may cause the trajectory sawtooth on the smooth sliding-mode surface.

Therefore, in order to reduce the system chattering, this paper proposes a hyperbolic tangent saturation function with an adjustable boundary layer $F(s)$ to replace the conventional sign(s) function, so that the sliding-mode variable is continuous, which further weakens the effect of chattering.

The hyperbolic tangent saturation function with adjustable boundary layer is expressed as

$$F(s) = \begin{cases} \mathrm{sign}(s) & |s| \geq \delta \\ \tanh(\lambda s) & |s| < \delta \end{cases} \tag{5}$$

where $\lambda = \pi\delta$, δ represents the thickness of the boundary layer. The bigger the thickness of the boundary layer is, the more obvious the chattering suppression is. However, too large the thickness of the boundary layer will affect the response speed of the sliding-mode soft switching and reduce the robustness of the system. Fig.2 shows the principle of the boundary layer thickness changing of the hyperbolic tangent function as the motor speed changes.

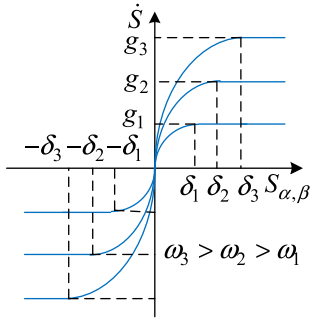

FIGURE 2. The principle of boundary layer variation of hyperbolic tangent function.

The saturation function $F(s)$ shown in (5) is used to replace the sign function in (4), so that switching control is used outside the boundary layer, and the linearized feedback control is used inside the boundary layer, which can restrain the chattering caused by sliding-mode switching to a certain extent. Therefore, the final expression of the NRL proposed

in this paper is

$$\begin{cases} \dot{s} = -k_1 H(x) F(s) - k_2 |x|^{\alpha} \cdot s \\ H(x) = \dfrac{|x|}{|x| + \varepsilon} \\ \lim\limits_{t \to \infty} |x| = 0, \quad k_1 > 0,\ k_2 > 0,\ 0 < \alpha < 2 \end{cases} \tag{6}$$

However, it needs to be noted that although the system chattering can be effectively reduced by using saturation function instead, the robustness of the system is sacrificed in a certain extent [24]. Therefore, other means are needed to enhance the immunity of the speed control system, which also provides a precondition for the introduction of the following disturbance observer.

C. NEW REACHING LAW CONTROL PERFORMANCE ANALYSIS

To make a comparative analysis among CERL, the reaching law in reference [9] (RLR9) and NRL, the typical motor system is given as

$$J\ddot{\theta} = u(t) + d(t) \tag{7}$$

where J is rotary inertia; $u(t)$ represents controller input; $\theta(t)$ is position instruction; $d(t)$ is external disturbance.

The controlled system is assumed to be

$$\ddot{\theta}(t) = -f(\theta, t) + gu(t) + d(t) \tag{8}$$

where θ is the feedback value of position. $f(\theta, t) = 25\,\dot{\theta}$ and $g = 133$; $d(t)$ is set as $10\sin(\pi t)$.

Assuming that θ_{d} is an ideal position signal, the error signal e can be expressed as $\theta_{\mathrm{d}} - \theta$. The surface function s is expressed as

$$s = \dot{e} + ce \tag{9}$$

where $c > 0$.

The position tracking error and its reciprocal can be defined as

$$\begin{cases} e(t) = \theta_{\mathrm{d}} - \theta(t) \\ \dot{e}(t) = \dot{\theta}_{\mathrm{d}} - \dot{\theta}(t) \end{cases} \tag{10}$$

where $\theta_{\mathrm{d}}(t)$ is ideal position signal.

Next, combining the (7), (8), (9) and (10), we can obtain that

$$\begin{aligned} \dot{s}(t) &= c\dot{e}(t) + \ddot{e}(t) \\ &= c(\dot{\theta}_{\mathrm{d}} - \dot{\theta}(t)) + (\ddot{\theta}_{\mathrm{d}} - \ddot{\theta}(t)) \\ &= c(\dot{\theta}_{\mathrm{d}} - \dot{\theta}(t)) + (\ddot{\theta}_{\mathrm{d}} + f(\theta, t) - gu - d) \end{aligned} \tag{11}$$

Using $F(s)$ instead of the sign(s), and combining the NRL with (12), the sliding-mode control law is expressed as

$$\begin{aligned} u(t) = \frac{1}{g}(k_1 H(x) F(x) + k_2 |x|^{\alpha} \cdot s \\ + c(\dot{\theta}_{\mathrm{d}} - \dot{\theta}) + \ddot{\theta} + f(\theta, t)) \end{aligned} \tag{12}$$

The simulation experiments are carried out among CERL, the reaching law in reference [9] (RLR9) and NRL using MATLAB s function. The simulation parameters are set as follows: $c = 15$, $k_1 = 10$, $k_2 = 50$, $\varepsilon = 1.5$, $\alpha = 1.2$. The ideal position signal θ_{d} is set as $\sin t$. The controlled object $\boldsymbol{x}(0)$ is set as $[x_1, x_2] = [-2, -2]$.

Fig.3 shows the performance comparison diagram among the CERL, RLR9 and NRL. We can conclude that the NRL is obviously superior to the CERL in tracking the given signal, reducing the position tracking error and suppressing the chattering. Compared with the reaching law in reference [9], the NRL proposed in this paper has the advantages of faster reaching speed and better stable controller output performance.

D. DESIGN OF SLIDING-MODE SPEED CONTROLLER BASED ON NRL

The role of the speed loop is to ensure that the system has the performance of restraining the speed fluctuation under the condition of parameter perturbation and external load disturbance, and can track the given speed quickly and accurately. In addition, the basic idea of the sliding-mode speed controller is to guide the state trajectory from any starting position to the sliding-mode surface by the reaching law control function, while ensuring that the system is progressively stable on the sliding-mode surface.

Therefore, in order to facilitate controller design, the state variables of the system are defined as

$$\begin{cases} x_1 = \omega^* - \omega \\ x_2 = \dot{\omega}^* - \dot{\omega} \end{cases} \tag{13}$$

where ω^* is a given reference speed and assumes that it is second-order differentiable, ω is the actual feedback speed.

According to the mathematical model of PMSM and (13), then

$$\begin{aligned} \dot{x}_2 &= \ddot{\omega}^* - \ddot{\omega} \\ &= -\frac{B}{J}x_2 - \frac{3p\psi_{\mathrm{f}}}{2J}\dot{i}_q + \frac{\dot{T}_L}{J} + \ddot{\omega}^* + \frac{B}{J}\dot{\omega}^* \end{aligned} \tag{14}$$

where L represents the equivalent inductance of the stator winding. p is the number of poles of the motor. J represents the motor moment of inertia. B is the viscous friction coefficient. Ψ_{f} is a permanent magnet flux linkage. $\dot{T}_{\mathrm{L}}$ represents the estimated load torque.

When considering the internal parameter perturbation of the system and the external load disturbance, (14) can be rewritten as

$$\begin{aligned} \dot{x}_2 = \left(-\frac{B}{J} + \Delta a\right) x_2 + \left(-\frac{3p\psi_{\mathrm{f}}}{2J} + \Delta b\right) \dot{i}_q \\ + \left(\frac{\dot{T}_L}{J} + \ddot{\omega}^* + \frac{B}{J}\dot{\omega}^* + \Delta c\right) \end{aligned} \tag{15}$$

where Δa, Δb, Δc are the uncertainties of the system corresponding terms.

If it is assumed that the system comprehensive disturbance amount is $R(t)$, which includes system internal parameter

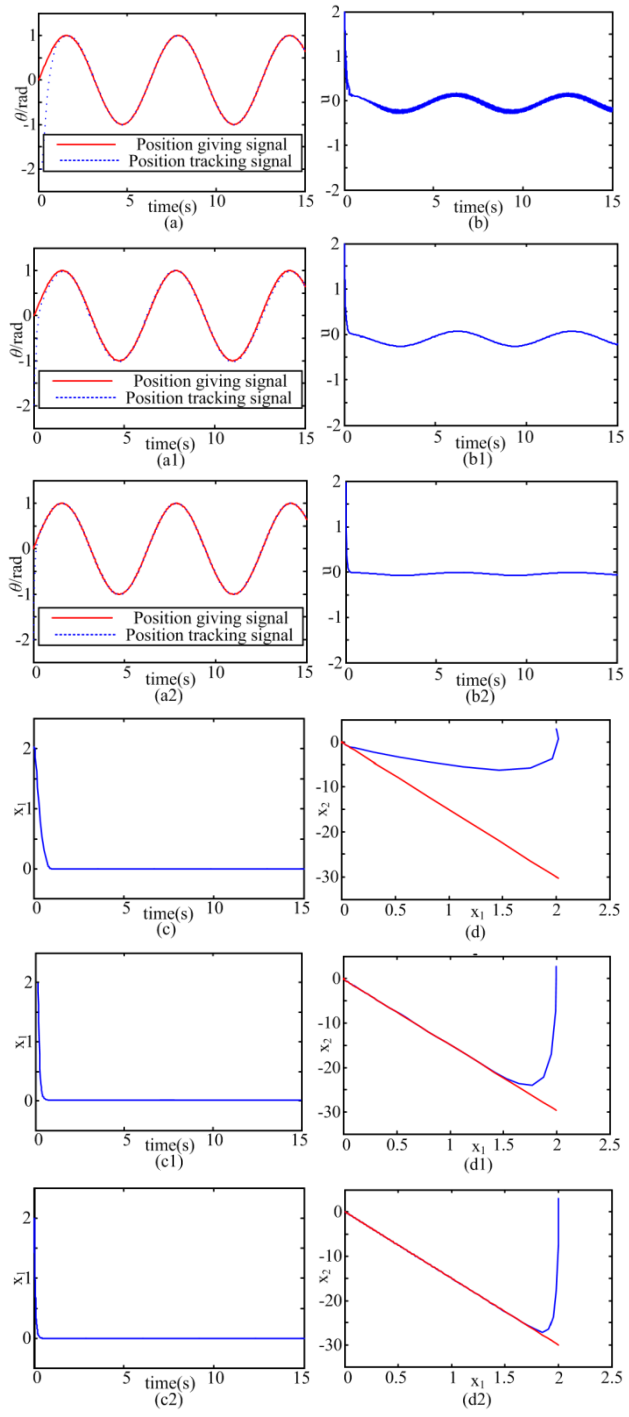

FIGURE 3. Performance comparison among different reaching laws (a) Tracking performance of CERL. (a1) Tracking performance of the RLR9. (a2) Tracking performance of NSMRL. (b) Controller output of CERL. (b1) Controller output of the RLR9 (b2) Controller output of NSMRL. (c) Position error convergence rate of CERL. (c1) Position error convergence rate of the RLR9. (c2) Position error convergence rate of NSMRL. (d) Phase trajectory of CERL. (d1) Phase trajectory of the RLR9. (d2) Phase trajectory of NSMRL.

perturbation and external load disturbance, etc., then $R(t)$ can be expressed as

$$R(t) = \Delta a x_2 + \Delta b \dot{i}_q + \left(\frac{\dot{T}_L}{J} + \ddot{\omega}^* + \frac{B}{J}\dot{\omega}^* + \Delta c \right) \quad (16)$$

Because the motor variables are bounded, the system's comprehensive disturbance satisfies the following equation

$$|R(t)| \le l_r \quad (17)$$

where l_r represents the limit value of the system comprehensive disturbance.

Considering $R(t)$ as the extended state variable of the system, combined with equations (13) and (16), the extended state equation of the system based on R(t) is

$$\begin{cases} \dot{x}_1 = x_2 \\ \dot{x}_2 = -Ax_2 - Du + R(t) \end{cases} \quad (18)$$

where $A = \frac{B}{J}$, $D = \frac{3p\Psi_f}{2J}$, $u = \dot{i}_q$.

Selecting the linear sliding-mode surface as shown in (19)

$$\begin{cases} s = cx_1 + x_2 \\ \dot{s} = (c - A)x_2 - Du + R(t) \end{cases} \quad (19)$$

where c is the design constant.

The speed controller is designed using the NRL proposed in this paper. It should be noted here that since the state variable x_1 is the speed tracking error, which is an important performance evaluation index for the speed control system, therefore, we choose x_1 as the state variable associated with the approaching speed. In this way, the error information is directly applied to the sliding-mode approaching speed to achieve the purpose of accelerating the approaching speed and suppressing the chattering.

In summary, choosing $x = x_1$ and combining (6) and (19), the equation shown in (20) can be obtained as

$$(c - A)x_2 - Du + R(t) = -k_1 H(x_1) F(s) - k_2 |x_1|^\alpha \cdot s \quad (20)$$

From equation (20), the output of the controller is

$$u = \frac{1}{D}\left[k_1 H(x_1) F(s) + k_2 |x_1|^\alpha \cdot s + (c - A)x_2 + R(t)\right] \quad (21)$$

Then the reference value of q-axis current can be obtained as

$$i_q^* = \frac{1}{D}\int \left[k_1 H(x_1) F(s) + k_2 |x_1|^\alpha \cdot s + (c - A)x_2 + R(t)\right] dt \quad (22)$$

The flow chart of the variable structure of the system control amount i_q^* is shown in Fig. 3. From the flow chart, the calculation process of reference value of q-axis current designed in this paper is relatively simple and easy to be realized by DSP software.

It can be seen from (22) and flow chart 4 that the disturbance term $R(t)$ has a great influence on the system control performance. Because in practical applications, the system disturbance can not be measured, and the minimum values of switching gain k_1 and k_2 will increase with the increase of disturbance. However, the increase of switching gain will aggravate the system chattering. Therefore, this paper chooses to add disturbance observer to observe the change of $R(t)$ in real time and compensate for it by a feedforward channel.

Only a small switching gain is needed to satisfy the robustness requirement of the system, and further weaken the chattering of the system.

E. PROOF OF STABILITY

To verify the stability of the designed sliding-mode speed controller, selecting the Lyapunov function as $V = s^2/2$. Drawing on reference book Lyapunov Stability Theory [27], when (23) is established, the condition of sliding-mode arrival can be satisfied.

$$\lim_{s\to 0} \dot{V} = \lim_{s\to 0} s\dot{s} \le 0 \tag{23}$$

Combining equations (6)and (19), then

$$\dot{V} = s\dot{s} = s\left[-k_1 H(x) F(s) - k_2 |x|^{\alpha} \cdot s\right] \tag{24}$$

From above equation, the following conclusion can be obtained

$$\begin{cases} -k_1 H(x_1)|s| - k_2 |x_1|^{\alpha} \cdot s^2 & |s| \ge \delta \\ -k_1 H(x_1)|\tanh|s| - k_2 |x_1|^{\alpha} \cdot s^2 & |s| < \delta \end{cases} \tag{25}$$

In (25), k_1 and k_2 are both constants greater than zero, and $|s|$ and $|x|$ are positive values. Therefore, Lyapunov stability condition can be satisfied. It is proved that the reaching law designed in this paper can guarantee the reachability of the sliding-mode motion of system state.

When the system state reaches the sliding-mode surface ($s = 0$), the system enters the sliding-mode control state. Combined with the system equation of state (18), the differential equation is obtained as follows

$$s = cx_1 + \dot{x}_1 = 0 \tag{26}$$

Solving the homogeneous linear differential equation of one variable, the equation (27) is obtained.

$$x_1 = \omega^* - \omega = C_0 e^{-ct} \tag{27}$$

where C_0 is a constant. With t increasing, x_1 tends to zero exponentially, which enables tracking without overshoot and allows the system to eventually reach a steady state.

III. DESIGN OF ANTI-DISTURBANCE SLIDING-MODE SPEED CONTROLLER BASED ON NRL

A. EXTENDED SLIDING-MODE DISTURBANCE OBSERVER (ESMDO) DESIGN

In order to solve the contradiction between chattering suppression and anti-disturbance ability in the sliding-mode control system, this paper designs an extended sliding-mode disturbance observer (ESMDO). Based on the conventional load torque observer, the simultaneous observation of the disturbance torque and the motor speed can be realized, and the observation results are compensated to the sliding-mode speed controller to achieve the purpose of further suppressing the system chattering. The structure diagram of the disturbance observer is shown in Figure 5.

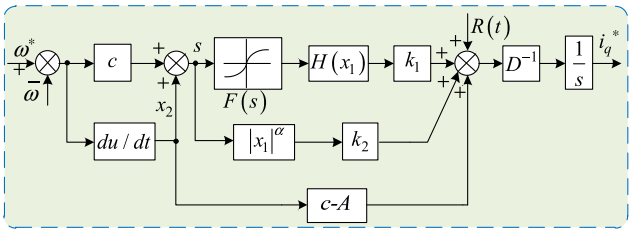

FIGURE 4. Variable structure flow chart of control variable i_q*.

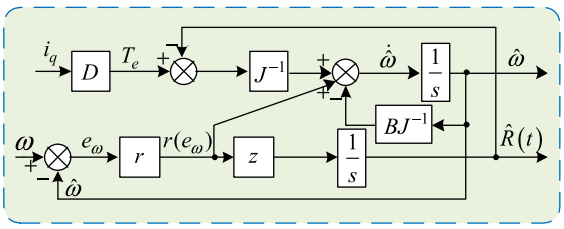

FIGURE 5. Structure diagram of sliding-mode disturbance observer.

Since the switching frequency of the controller is usually high, it can be considered that the load torque is constant within one controller cycle, that is $\dot{T}_L = 0$.

The motor speed ω and the system comprehensive disturbance amount $R(t)$ are selected as the state variables, and the electromagnetic torque T_e is used as the system input, and the motor speed ω is used as the system output, then the extended state space equation can be expressed as

$$\begin{bmatrix} \dot{\omega} \\ \dot{R}(t) \end{bmatrix} = \begin{bmatrix} -\frac{B}{J} & -\frac{1}{J} \\ 0 & 0 \end{bmatrix} \begin{bmatrix} \omega \\ R(t) \end{bmatrix} + \begin{bmatrix} \frac{1}{J} \\ 0 \end{bmatrix} T_e \tag{28}$$

Taking the motor speed and the system comprehensive disturbance amount $R(t)$ as the observation object, the equation of the sliding-mode disturbance observer obtained by (28) is

$$\begin{bmatrix} \dot{\hat{\omega}} \\ \dot{\hat{R}}(t) \end{bmatrix} = \begin{bmatrix} -\frac{B}{J} & -\frac{1}{J} \\ 0 & 0 \end{bmatrix} \begin{bmatrix} \hat{\omega} \\ \hat{R}(t) \end{bmatrix} + \begin{bmatrix} \frac{1}{J} \\ 0 \end{bmatrix} T_e + \begin{bmatrix} 1 \\ z \end{bmatrix} r(\omega_e) \tag{29}$$

where $r(\omega_e)$ is the sliding-mode control rate of the observation error $e_\omega = \omega^* - \hat{\omega}$, and z is the observer gain.

Then, combining equations (28) and (29), the error equation of the observer can be written as

$$\begin{cases} \dot{e}_\omega = -\frac{B}{J} e_\omega - \frac{1}{J} e_R - r(e_\omega) \\ \dot{e}_R = -z r(e_\omega) \end{cases} \tag{30}$$

where e_ω, e_R represent the motor speed and disturbance observation error, respectively.

Selecting the integral sliding-mode surface as

$$s_\omega = e_\omega + c_\omega \int_0^t e_\omega dt \tag{31}$$

If deriving equation (31), there is $\dot{s}_\omega = \dot{e}_\omega + c_\omega e_\omega$, then, the sliding-mode reaching law, as written by

$$\dot{s}_\omega = -k_3 \text{sign}(s) \tag{32}$$

where k_3 represents the sliding-mode switching gain.

Combining equations (31) and (32), and using $-e_R/J$ as the disturbance term, the control law of the ESMDO is given by

$$r(e_\omega) = \left(c_\omega - \frac{B}{J}\right) e_\omega + k_3 \text{sign}(s_\omega) \tag{33}$$

Under the action of the sliding-mode control law, the system trajectory finally reaches the sliding-mode surface and enters the sliding-mode state, then, the following equations can be obtained

$$\begin{cases} s_\omega = \dot{s}_\omega = 0 \\ e_\omega = \dot{e}_\omega = 0 \end{cases} \tag{34}$$

Combining equations (30) and (34), then

$$\begin{cases} e_R = -Jr(e_\omega) \\ \dot{e}_R = -zr(e_\omega) \end{cases} \tag{35}$$

Solving the equation (35) can get the following result

$$e_R = c_R e^{\frac{z}{J}t} \tag{36}$$

where c_R is a constant.

It can be seen from (36) that in order to make the error of disturbance observer converge to zero, the parameter z needs to satisfy $z < 0$. At this time, the convergence speed of ESMDO is completely determined by the value of z.

B. ANTI-DISTURBANCE SLIDING-MODE SPEED CONTROLLER BASED ON NRL

The load disturbance value $\hat{R}(t)$ obtained by the disturbance observer is compensated at the output of the SMSC, and the SMSC is obtained by rewriting (22), as described by

$$i_q^* = \frac{1}{D}\int \left[k_1 H(x_1) F(s) + k_2 |x_1|^\alpha \cdot s + (c-A) x_2 + \hat{R}(t)\right] dt \tag{37}$$

In summary, the structure diagram of the obtained anti-disturbance PMSM sliding-mode speed control based on the NRL and considering the system comprehensive disturbance is shown in Fig. 6.

According to Fig. 6, the anti-disturbance sliding-mode controller proposed in this paper consists of two parts: the first part is a SMSC based on a NRL, which is shown in Part I of the Fig. 6; the second part is a disturbance observation compensation link based on an ESMDO, which is shown in part II of Fig. 6.

It can be seen from the figure that the system disturbance is fed back to the SMSC with a known amount. Therefore, when the system load disturbance occurs, the controller can respond to the torque change in time, so that it can achieve better anti-disturbance performance without large control gain. In addition, the Anti-disturbing and robustness improving performance also weaken the system chattering in a certain extent.

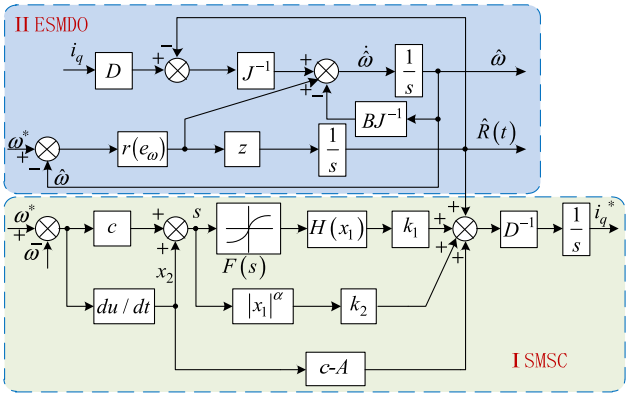

FIGURE 6. Structural diagram of Anti-disturbance sliding-mode controller based on NRL.

C. PROOF OF SYSTEM STABILITY

In order to verify the stability of the servo system under the control method SMSC+ESMDO, the Lyapunov function is chosen as $V = s^2/2$. According to the stability criterion, the controlled system is asymptotically stable when the equation (38) is established.

$$\frac{dV}{dt} = s \cdot \dot{s} \le 0 \tag{38}$$

Combining equations (19) and (37), then

$$\dot{s} = -k_1 H(x_1) F(s) - k_2 |x_1|^\alpha \cdot s + \left(R(t) - \hat{R}(t)\right) \tag{39}$$

According to equations (38) and (39), it can be obtained that

$$s\dot{s} = S\left[-k_1 H(x) F(s) - k_2 |x|^\alpha \cdot s\right] + \left|R(t) - \hat{R}(t)\right| \cdot |s| \tag{40}$$

Because the stability of the disturbance observer proves that $\left|R(t) - \hat{R}(t)\right| \to 0$, when k_2 is large enough, it can satisfy $s \cdot \dot{s} \le 0$, thus satisfying the stability requirement.

IV. SIMULATION AND EXPERIMENTAL VERIFICATION

In order to further verify the performance of the new approaching SMSC based on the extended state observer, the PMSM vector control system structure with $i_d = 0$ is used, and the simulation model is built by Matlab/Simulink. In the simulation, the motor parameters are set as Table 1.

TABLE 1. Parameters of the motor.

Parameter and unit	Value
Rated power P_n/kW	0.4
Inductance $L_d = L_q$/mH	6.71
Flux linkage of permanent magnets Ψ_a/Wb	0.175
Stator phase resistance R/Ω	1.55
Viscous friction coefficient B/N·m·s	0.000 3
Rotational inertia J/kg·m^2	0.000 2

A. SIMULATION VERIFICATION

As can be seen from the simulation block diagram of PMSM servo system based on SMSC+ESMDO shown in Fig. 7,

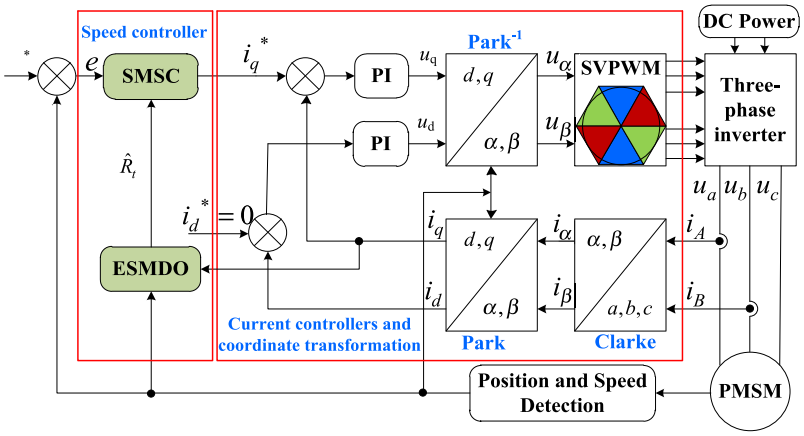

FIGURE 7. Block diagram of PMSM speed-regulation system.

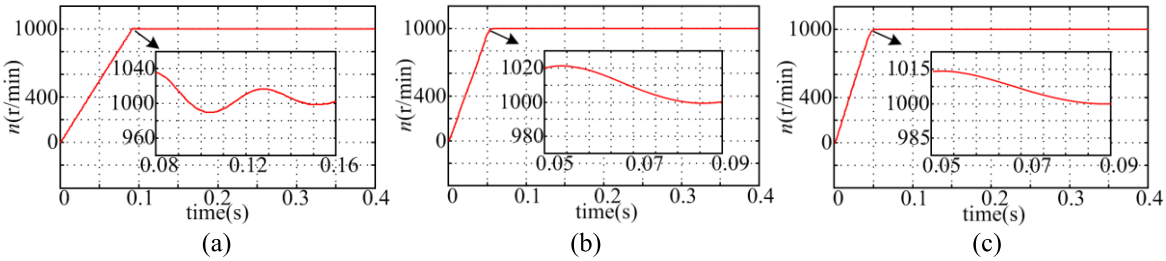

FIGURE 8. Start comparison simulations under different control strategies. (a) Simulation results under PI controller. (b) Simulation results under SMSC using the reaching law in Ref.9 (RLR9). (c) Simulation results under SMSC using NRL.

the ESMDO estimates the load disturbance of the system and compensates the results to SMSC, while the SMSC replaces the PI controller in the conventional speed loop. In addition, Clarke and Parke transform realize the transformation from A-B-C frame to α-β frame, and the transformation from α-β frame to d-q frame respectively.

It should be noted that, when using the standard PI algorithm as the speed controller for comparison here, an antiwindup PI algorithm [28] is employed here for the speed loop. The main idea of this antiwindup strategy can be described as follows

$$e_1(k) = \omega_r^*(k) - \omega_r(k) \tag{41}$$

If $i_q^*(k-1) > I_{q\max}$, then

$$\alpha = \begin{cases} 0, & e_1(k) > 0 \\ 1, & e_1(k) < 0 \end{cases} \tag{42}$$

If $i_q^*(k-1) < -I_{q\max}$, then

$$\alpha = \begin{cases} 0, & e_1(k) < 0 \\ 1, & e_1(k) > 0 \end{cases} \tag{43}$$

If $-I_{q\max} \le i_q^*(k-1) \le I_{q\max}$, then $\alpha = 1$.

$$i_q^*(k) = \mathrm{k}_p * e_1(k) + k_i * \sum_{i=0}^{k} \alpha e_1(k) \tag{44}$$

In order to verify the dynamic performance of NRL, the first simulation has presented the starting response of different control strategies (PI, SMSC using the reaching law in Ref.9, SMSC using NRL) when the system is no-load starting. The simulation time t is set to 0.4 s, the motor starting load torque is 0 N·m, and the given speed is 1000 r/min. The first simulation results are shown in Fig. 8.

To verify the dynamic response and robustness performance of the PMSM control system, the motor starting load torque is set as 0.2 N·m. When running to 0.2 s, the load torque is suddenly increased to 1.27 N·m. At 0.3 s, the load torque is suddenly discharged to 0.7 N·m. The simulation results are shown in Fig. 9 to Fig. 11.

The PI parameters of both current loops are the same as: $k_{\mathrm{pc}} = 0.8$, $k_{\mathrm{ic}} = 0.05$. The PI parameters of the speed loop is that proportional gain $k_{\mathrm{p}} = 0.25$, and the integral gain $k_{\mathrm{i}} = 17$, $\alpha_0 = 0.998$. The parameters of the SMSC+ESMDO controller are: $k_1 = 10$, $k_2 = 50$, $\alpha = 1.2$, $\varepsilon = 1.5$, $x = x_1$, $\delta = 0.3$, $c = 15$, $z = 3$, $l_{\mathrm{r}} = 30$, $m = 1.5$.

We can draw the following conclusions from the simulation results shown in Fig.8. Compared to the servo system controlled by PI algorithm shown in Fig.8(a), the servo system using the SMSC based on the NRL shown in Fig.8(c) has shorter time to reach the stable running state, and achieves the steady state almost without overshoots, while the servo system under PI control has an overshoot. Comparing Fig.8(c) and Fig.8(b), it can be seen that SMSC using NRL achieves

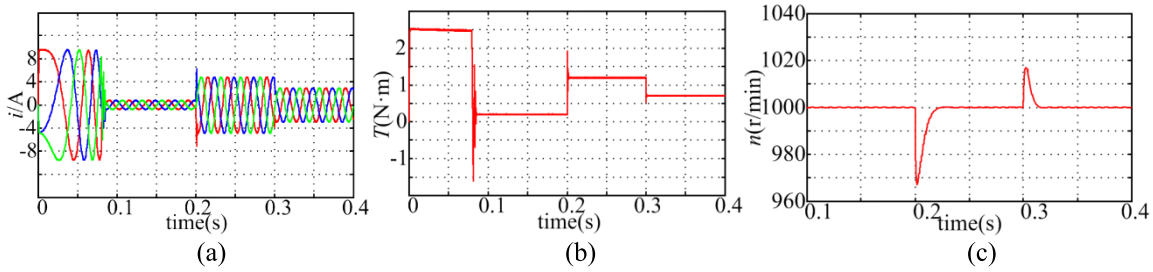

FIGURE 9. Simulation results of dynamic response of load mutation under PI control. (a) Three-phase current (b) Torque change in the case of load disturbances (c) Speed fluctuation in the case of load disturbances.

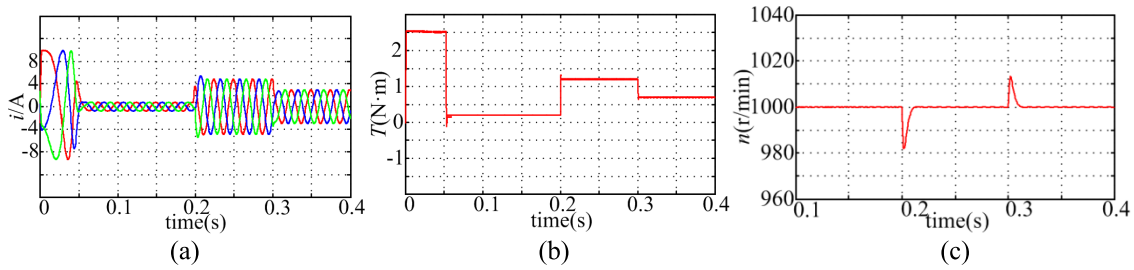

FIGURE 10. Simulation results of dynamic response of load mutation under SMSC adopting NRL. (a) Three-phase current (b) Torque change in the case of load disturbances (c) Speed fluctuation in the case of load disturbances.

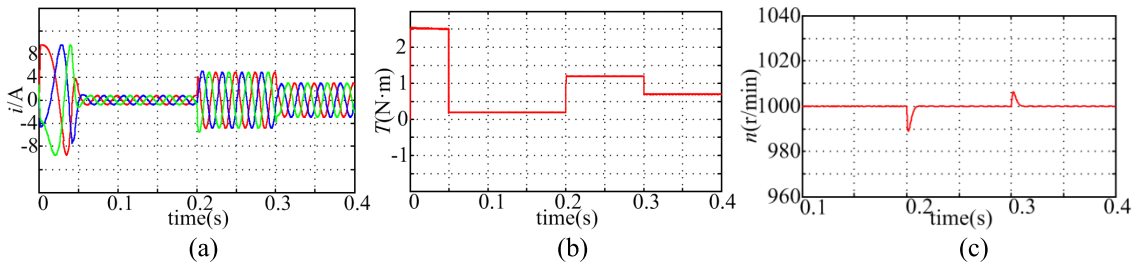

FIGURE 11. Simulation results of dynamic response of load mutation under SMSC+ESMDO. (a) Three-phase current (b) Torque change in the case of load disturbances (c) Speed fluctuation in the case of load disturbances.

the given speed in a shorter time than SMSC using the reaching law in Ref.9 (RLR9).

As shown in Fig.9(a)–(c) under PI controller, it can be seen that when the external disturbance is applied, the servo system is sensitive to the load torque changes, the stator current distortion is severe, and the error of motor speed is about 30 r/min.

In contrast, as shown in Fig.10(a)–(c), when using the NRL-based SMSC controller, the speed and torque of the PMSM control system have better dynamic performance. The electromagnetic torque has almost no fluctuations, and the motor speed change is smaller, less than 20 r/min. More importantly, there is nearly no speed fluctuations in the stable speed stage.

Compared with Fig.10 and Fig.11, it can be found that when the control mode of SMSC+ESMDO is adopted, the change value of speed is smaller shown in Fig.11(c) when the load torque suddenly increase or decrease, which indicates that the robustness of the system is further improved effectively.

Therefore, we can draw the conclusion that the system with the NRL-based SMSC+ESMDO controller has the advantages of good dynamic ability and strong robustness from the above analysis.

B. EXPERIMENTAL VERIFICATION

To further verify the proposed control method, a PMSM experiment platform based on TMS320F28335 was set up [29]. The experiment mainly verifies the dynamic response of the servo system under the PI controller, the SMSC controller, and the proposed SMSC+ESMDO controller. Fig.12 is the experiment hardware platform.

The PI parameters of the two current loops are the same: the proportional gain $k_{pc} = 0.77$, and the integral gain $k_{ic} = 0.05$. The PI parameters of the speed loop is that proportional gain $k_p = 0.25$, and the integral gain $k_i = 20$, $\alpha_0 = 0.998$. The parameters of SMSC+ESMDO are: $k_1 = 9.7$, $k_2 = 55$, $\alpha = 1.2$, $\varepsilon = 1.5$, $x = x_1$, $\delta = 0.5$, $c = 15$, $z = 3$, $l_r = 30$, $m = 1.5$. The parameters of the

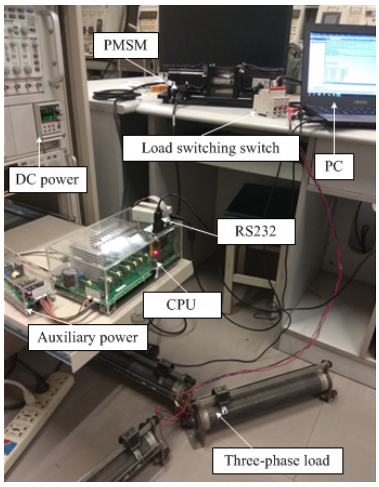

FIGURE 12. Experimental hardware platform.

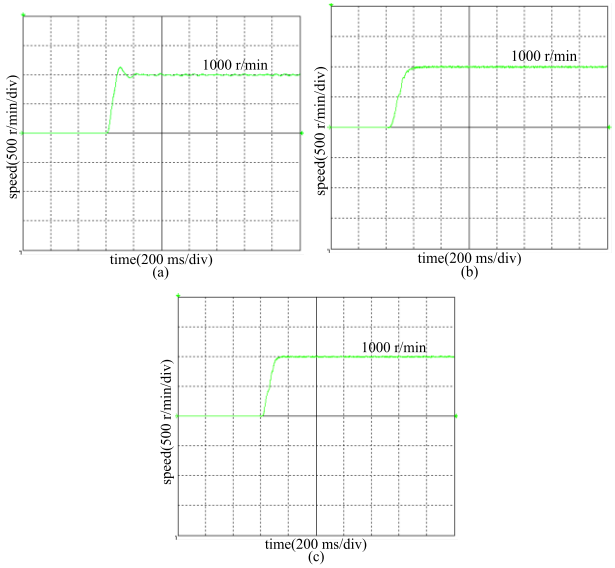

FIGURE 13. Start comparison experiments under different control strategies. (a) Experiment results under PI controller. (b) Experiment results under SMSC using the reaching law in Ref.9 (RLR9). (c) Experiment results under SMSC using NRL.

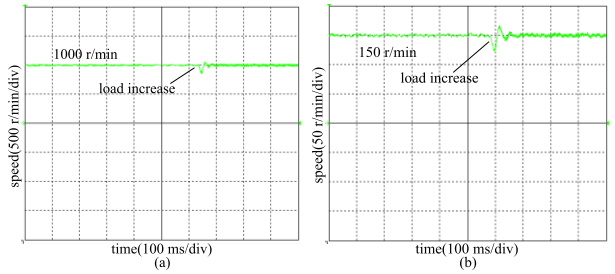

FIGURE 14. Experimental results under PI controller. (a) Speed (1000 r/min) in the case of sudden load increase. (b) Speed (150 r/min) in the case of sudden load increase.

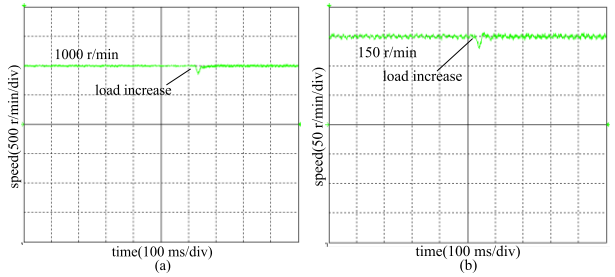

FIGURE 15. Experimental results under SMSC adopting NRL. (a) Speed (1000 r/min) in the case of sudden load increase. (b) Speed (150 r/min) in the case of sudden load increase.

experimental PMSM are as follows: rated speed 3 000r/min, rated power 0.4kW, rated torque 1.27 N·m.

In order to verify the dynamic performance of NRL, the first experiment has presented the starting response with different control strategies when the system is under no-load operation.

The starting comparison experiment results under different control strategies (i.e., PI, SMSC+RLR9, SMSC+NRL) are shown in Fig.13 (a)–(c). When the PMSM is started with a given speed of 1000 r/min, compared with Fig.13 (a) and Fig.13 (b), (c), when the PI controller is used, the starting speed fluctuation is very obvious, about 150r/min. Besides, the dynamic settling time is about 250 ms, which is longer than when using SMSC. In addition, combined with the experimental results of Fig.13 (b) and (c), we can see that the starting speed of the system has almost no overshoot after using the NRL. Moreover, the speed settling time is shorter than adopting the reaching law in RLR9. Therefore, from the experimental results shown in Fig. 13, it can be seen that the dynamic performance of the controlled PMSM servo system is effectively improved when the NRL designed in this paper is adopted.

Then, when the PMSM is running at a steady speed of 1000 r/min and at a low speed of 150 r/min, the second experiment has been implemented to verify the robustness of the three control strategies (PI, SMSC, SMSC+ESMDO). Fig.14, Fig.15and Fig.16 show the speed dynamic responses when a 1.27 N·m load torque is added suddenly.

From Fig.14 (a) and Fig.15 (a), it can be see that when the 1.27 N·m load torque is added suddenly, the speed fluctuation in PI control is about 100 r/min. The dynamic settling time is about 80 ms. Relatively, as shown in Fig.15 (a), using the method of SMSC, when the load torque is changed suddenly, the speed fluctuation of the PMSM system is small, about 80 r/min. Moreover, its dynamic settling time is shorter. When the load torque is increased 1.27 N·m suddenly at 150 r/min, the same conclusion can still be obtained from the experimental results Fig.14 (b) and Fig.15(b).

In addition, from the results of Fig.16, it can be see that the method of SMSC+ESMDO has satisfying disturbance suppression ability compared with other methods. Whether at the high speed of 1000 r/min or at the low speed of 150 r/min, the fluctuation of speed under sudden load

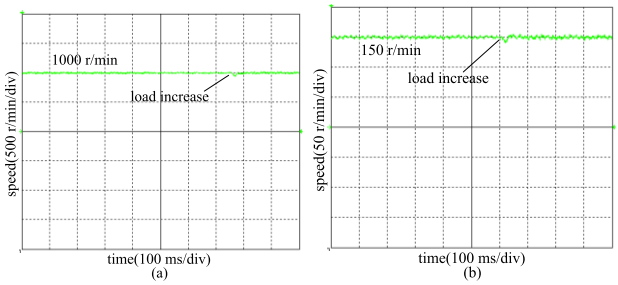

FIGURE 16. Experimental results under SMSC+ESMDO. (a) Speed (1000 r/min) in the case of sudden load increase. (b) Speed (150 r/min) in the case of sudden load increase.

change is about 30 r/min and 10 r/min, respectively, which are smaller than that of the first two control strategies. Therefore, the SMSC+ESMDO control method proposed in this paper can effectively enhance the robustness of the controlled motor servo system.

V. CONCLUSION

In this paper, a composite sliding-mode control strategy is proposed and has been experimentally applied to the PMSM system. The major contributions of this paper include: 1) a speed controller based on a NRL is proposed for PMSM; 2) an extended state observer based on hyperbolic tangent function is designed to estimate the load disturbance; 3) a composite control method that combines SMSC and ESMDO is developed to further improve the disturbance rejection ability of SMSC system. The superiority of the proposed method SMSC+ESMDO has been confirmed through simulations and experiments, which results show that the designed method can effectively improve the dynamic performance and robustness of the PMSM servo system.

REFERENCES

[1] Q. Yang, Z. Kang, M. Zhang, and N. Zhao, "Study on space vector PWM technology of PMSM control system based on dSPACE," in *Proc. IEEE Int. Conf. Inf. Automat. (ICIA)*, Yinchuan, China, Aug. 2013, pp. 576–580.
[2] Z. Xiaoguang, Z. Ke, and S. Li, "A PMSM sliding mode control system based on a novel reaching law," in *Proc. Int. Conf. Elect. Mach. Syst.*, Aug. 2011, pp. 1–5.
[3] S. Li and Z. Liu, "Adaptive speed control for permanent-magnet synchronous motor system with variations of load inertia," *IEEE Trans. Ind. Electron.*, vol. 56, no. 8, pp. 3050–3059, Aug. 2009.
[4] D. Liang, J. Li, and R. Qu, "Sensorless control of permanent magnet synchronous machine based on second-order sliding-mode observer with Online resistance estimation," *IEEE Trans. Ind. Appl.*, vol. 53, no. 4, pp. 3672–3682, Jul./Aug. 2017.
[5] Y. S. Kung and M. H. Tsai, "FPGA-Based Speed Control IC for PMSM Drive With Adaptive Fuzzy Control," *IEEE Trans. Power Electron.*, vol. 22, no. 6, pp. 2476–2486, Nov. 2007.
[6] X. Sun, C. Hu, G. Lei, Y. Guo, and J. Zhu, "State feedback control for a PM hub motor based on gray wolf optimization algorithm," *IEEE Trans. Power Electron.*, vol. 35, no. 1, pp. 1136–1146, Jan. 2020, doi: 10.1109/TPEL.2019.2923726.
[7] Z. Mynar, L. Vesely, and P. Vaclavek, "PMSM model predictive control with field-weakening implementation," *IEEE Trans. Ind. Electron.*, vol. 63, no. 8, pp. 5156–5166, Aug. 2016.
[8] X. Sun, Z. Shi, L. Chen, and Z. Yang, "Internal model control for a bearingless permanent magnet synchronous motor based on inverse system method," *IEEE Trans. Energy Convers.*, vol. 31, no. 4, pp. 1539–1548, Dec. 2016.
[9] X. Zhang, L. Sun, K. Zhao, and L. Sun, "Nonlinear speed control for PMSM system using sliding-mode control and disturbance compensation techniques," *IEEE Trans. Power Electron.*, vol. 28, no. 3, pp. 1358–1365, Mar. 2013.
[10] V. Repecho, D. Biel, and A. Arias, "Fixed switching period discrete-time sliding mode current control of a PMSM," *IEEE Trans. Ind. Electron.*, vol. 65, no. 3, pp. 2039–2048, Mar. 2018.
[11] C. Mu, W. Xu, and C. Sun, "On switching manifold design for terminal sliding mode control," *J. Franklin Inst.*, vol. 353, no. 7, pp. 1553–1572, May 2016.
[12] X. Sun, L. Chen, Z. Yang, and H. Zhu, "Speed-sensorless vector control of a bearingless induction motor with artificial neural network inverse speed observer," *IEEE/ASME Trans. Mechatronics*, vol. 18, no. 4, pp. 1357–1366, Aug. 2013.
[13] L. Saihi, A. Bouhenna, M. Chenafa, and A. Mansouri, "A robust sensorless SMC of PMSM based on sliding mode observer and extended Kalman filter," in *Proc. 4th Int. Conf. Electr. Eng. (ICEE)*, Boumerdes, Algeria, Dec. 2015, pp. 1–4.
[14] L. Chai and F. Yao, "Sliding mode control with friction observer and load observer of PMSM," in *Proc. 15th Int. Conf. Control, Autom. Syst. (ICCAS)*, Busan, South Korea, Oct. 2015, pp. 1102–1106.
[15] C.-K. Lai and K.-K. Shyu, "A novel motor drive design for incremental motion system via sliding-mode control method," *IEEE Trans. Ind. Electron.*, vol. 52, no. 2, pp. 499–507, Apr. 2005.
[16] Y. Feng, X. Yu, and F. Han, "High-order terminal sliding-mode observer for parameter estimation of a permanent-magnet synchronous motor," *IEEE Trans. Ind. Electron.*, vol. 60, no. 10, pp. 4272–4280, Oct. 2013.
[17] V. Q. Leu, H. H. Choi, and J.-W. Jung, "Fuzzy sliding mode speed controller for PM synchronous motors with a load torque observer," *IEEE Trans. Power Electron.*, vol. 27, no. 3, pp. 1530–1539, Mar. 2012.
[18] Y. Wang, Y. Feng, X. Zhang, and J. Liang, "A new reaching law for anti-disturbance sliding-mode control of PMSM speed regulation system," *IEEE Trans. Power Electron.*, to be published, doi: 10.1109/TPEL.2019.2933613.
[19] J. Ma, J. Zhao, J. Sun, and C. Yan, "A novel PMSM speed control scheme based on sliding-mode and fuzzy disturbance observer," in *Proc. 43rd Annu. Conf. IEEE Ind. Electron. Soc.*, Beijing, China, Oct./Nov. 2017, pp. 1704–1710.
[20] O. Kaynak, K. Erbatur, and M. Ertugnrl, "The fusion of computationally intelligent methodologies and sliding-mode control-a survey," *IEEE Trans. Ind. Electron.*, vol. 48, no. 1, pp. 4–17, Feb. 2001.
[21] A. Šabanovic, "Variable structure systems with sliding modes in motion control—A survey," *IEEE Trans. Ind. Informat.*, vol. 7, no. 2, pp. 212–223, May 2011.
[22] C. J. Fallaha, M. Saad, H. Y. Kanaan, and K. Al-Haddad, "Sliding-mode robot control with exponential reaching law," *IEEE Trans. Ind. Electron.*, vol. 58, no. 2, pp. 600–610, May 2011.
[23] C. Mu and H. He, "Dynamic behavior of terminal sliding mode control," *IEEE Trans. Ind. Electron.*, vol. 65, no. 4, pp. 3480–3490, Apr. 2018.
[24] M. A. M. Cheema, J. E. Fletcher, M. Farshadnia, D. Xiao, and M. F. Rahman, "Combined speed and direct thrust force control of linear permanent-magnet synchronous motors with sensorless speed estimation using a sliding-mode control with integral action," *IEEE Trans. Ind. Electron.*, vol. 64, no. 5, pp. 3489–3501, May 2017.
[25] S. Li, M. Zhou, and X. Yu, "Design and implementation of terminal sliding mode control method for PMSM speed regulation system," *IEEE Trans. Ind. Informat.*, vol. 9, no. 4, pp. 1879–1891, Nov. 2013.
[26] W. Gao and J. C. Hung, "Variable structure control of nonlinear systems: A new approach," *IEEE Trans. Ind. Electron.*, vol. 40, no. 1, pp. 45–55, Feb. 1993.
[27] H.-D. Chiang, "Lyapunov stability and stability regions of nonlinear dynamical systems," in *Direct Methods for Stability Analysis of Electric Power Systems: Theoretical Foundation, BCU Methodologies, and Applications*. Hoboken, NJ, USA: Wiley, 2011.
[28] A. S. Hodel and C. E. Hall, "Variable-structure PID control to prevent integrator windup," *IEEE Trans. Ind. Electron.*, vol. 48, no. 2, pp. 442–451, Apr. 2001.
[29] X. Sun, C. Hu, J. Zhu, S. Wang, W. Zhou, Z. Yang, G. Lei, K. Li, B. Zhu, and Y. Guo, "MPTC for PMSMs of EVs with multi-motor driven system considering optimal energy allocation," *IEEE Trans. Magn.*, vol. 55, no. 7, Jul. 2019, Art. no. 8104306.

YAOQIANG WANG (S'12–M'16) received the B.Sc. degree in measurement and control technology and instruments from Hangzhou Dianzi University, Hangzhou, China, in 2006, and the M.Sc. and Ph.D. degrees in electrical engineering from the Harbin Institute of Technology, Harbin, China, in 2008 and 2013, respectively.

He is currently working as an Associate Professor with the School of Electrical Engineering, Zhengzhou University, Zhengzhou, China. He has authored more than 30 technical articles published in journals and conference proceedings. His research interests include power conversion and control technique, and its applications in distributed generation, motor drive, as well as flexible power transmission and distribution.

YUTAO FENG received the B.Sc. degree in electrical engineering and its automation from the Shandong University of Science and Technology, Qingdao, China, in 2016, and the M.Sc. degree in electrical engineering from Zhengzhou University, Zhengzhou, China, in 2019.

He is currently working as a Researcher with the AVIC Jonhon Optronic Technology Company, Ltd., Luoyang, China. His research interests include power electronics and electric machine drives.

XIAOGUANG ZHANG (M'15) received the B.Sc. degree in electrical engineering from the Heilongjiang Institute of Technology, Harbin, China, in 2007, and the M.Sc. and Ph.D. degrees in electrical engineering from the Harbin Institute of Technology, Harbin, in 2009 and 2014, respectively.

From 2012 to 2013, he was a Research Associate with Wisconsin Electric Machines and Power Electronics Consortium (WEMPEC), University of Wisconsin–Madison, Madison. He is currently a Distinguished Professor with the North China University of Technology, Beijing, China. He has published more than 40 technical articles in the area of motor drives. His current research interests include power electronics and electric machine drives.

JUN LIANG (M'02–SM'12) received the B.Sc. degree from the Huazhong University of Science and Technology, Wuhan, China, in 1992, and the M.Sc. and Ph.D. degrees from the China Electric Power Research Institute (CEPRI), Beijing, China, in 1995 and 1998, respectively, all in electrical engineering and its automation.

From 1998 to 2001, he was a Senior Engineer with CEPRI. From 2001 to 2005, he was a Research Associate with Imperial College London, London, U.K. From 2005 to 2007, he was with the University of Glamorgan as a Senior Lecturer. He is currently a Professor with the School of Engineering, Cardiff University, Cardiff, U.K. He has been appointed as an Adjunct Professor with Zhengzhou University, Zhengzhou, China, since 2019. His research interests include power system stability and control, DC grids, power electronics, and renewable power generation.

XIAN CHENG received the Ph.D. degree in electrical engineering from the Dalian University of Technology, Dalian, China, in 2012.

He is currently working as an Associate Professor with the School of Electrical Engineering, Zhengzhou University, Zhengzhou, China. His research interests include power electronics, hybrid circuit breakers, and intellectual apparatus.